IJCRT.ORG ISSN : 2320-2882

INTERNATIONAL JOURNAL OF CREATIVE RESEARCH THOUGHTS (IJCRT)

An International Open Access, Peer-reviewed, Refereed Journal

Behavior And Capacity Prediction Of Partially Concrete-Filled Double-Skin Sections (PCFDS) Under Longitudinal And Transverse Filling Variations

Peter E. Amin, Ahmed M.Ibrahim*, Sherif K. Hassan

Department of Structural Engineering, Ain-Shams University, Cairo, Egypt

Keywords

Steel, concrete-filled, concrete-filled double skin, partially concrete-filled double skin.

Highlights

- Developed numerical models were validated against previous experimental studies and existing code equations, demonstrating good agreement and reliability.
- A comprehensive parametric study was conducted, varying diameter-to-thickness (D/t) ratios, longitudinal filling ratios, and transverse filling ratios to analyze their impact on structural behavior.
- Design equations were proposed to predict load-carrying capacity at different filling percentages, providing practical guidelines for the design of partially filled CFDST beams.

Abstract

The integration of steel and concrete properties offers significant advantages for structural elements, enhancing their strength and performance. This study focuses on partially filled concrete-filled double-skin tubular (CFDST) columns, investigating the longitudinal filling of concrete. Numerical models were developed and validated against previous experimental studies and existing code equations, demonstrating good agreement. A parametric study was conducted, incorporating numerical models with varying diameter-to-thickness (D/t) ratios, longitudinal filling ratios, and transverse filling ratios. The impact of longitudinal partial filling on the structural behavior was thoroughly analyzed, and design equations were proposed to predict the load-carrying capacity at different filling percentages.

1. Introduction

The combination of steel and concrete properties has consistently proven advantageous for structural elements, offering enhanced strength, stiffness, and durability. In a world where renewable energy and sustainability are essential, the demand for economical and efficient structural sections has become a priority.

Hollow steel sections (HSS) have emerged as a versatile solution over the past decades, offering several benefits, including symmetry, the absence of weak axes, lightweight properties, and simplified connections. These features make HSS an attractive choice for various structural applications. However, continuous advancements in their design have led to the development of concrete-filled sections (CFS), where concrete is added inside the hollow steel section. This innovation improves the stiffness and rigidity of the section while significantly enhancing its local buckling strength.

The behavior of CFS under bending was extensively studied by Moon et al. [1], while Lu et al. [2] examined the effect of thin steel walls. Khalifa et al. [3] explored the concept of partial longitudinal filling with concrete, and design equations for CFS capacity were included in AISC 360-10 [4]

Despite their advantages, the heavy weight of concrete in traditional CFS prompted researchers to investigate concrete-filled double-skin (CFDS) sections. CFDS sections consist of an inner and outer steel skin with concrete confined between them. This configuration retains the beneficial properties of concrete while significantly reducing the overall weight, resulting in a higher strength-to-weight ratio.

The behavior of CFDS sections has been widely studied. Tao and Han [5] examined their performance under compression for stub column specimens, while their bending behavior was analyzed experimentally, leading to the development of design equations to predict section capacity. Additionally, Huang et al. [6] investigated CFDS behavior under pure torsion, further expanding the understanding of these innovative structural elements.

Wind turbines and advertising signages are two prominent applications where hollow sections are extensively used. However, before the introduction of concrete-filled sections (CFS) and concrete-filled double-skin sections (CFDS), the weight of purely steel sections in such designs was significantly higher, making them less efficient compared to designs that incorporate concrete.

This thesis aims to investigate the partial filling of concrete in tubular sections to reduce the overall weight while increasing the strength-to-weight ratio. The study focuses on identifying the optimum concrete filling ratio in both transverse (Figure 1) and longitudinal (Figure 2) directions. Numerical models were developed to analyze the effects of varying longitudinal filling ratios in combination with different transverse filling ratios. The goal was to determine the governing failure modes, evaluate their interactions, and identify the critical failure mechanisms.

To achieve this, finite element analysis (FEA) was employed to study tubular sections with different diameter-to-thickness (D/t) ratios. The study also explored the influence of these parameters on structural performance and design limitations, providing insights into the potential failure types that may govern the behavior of these partially filled tubular sections.

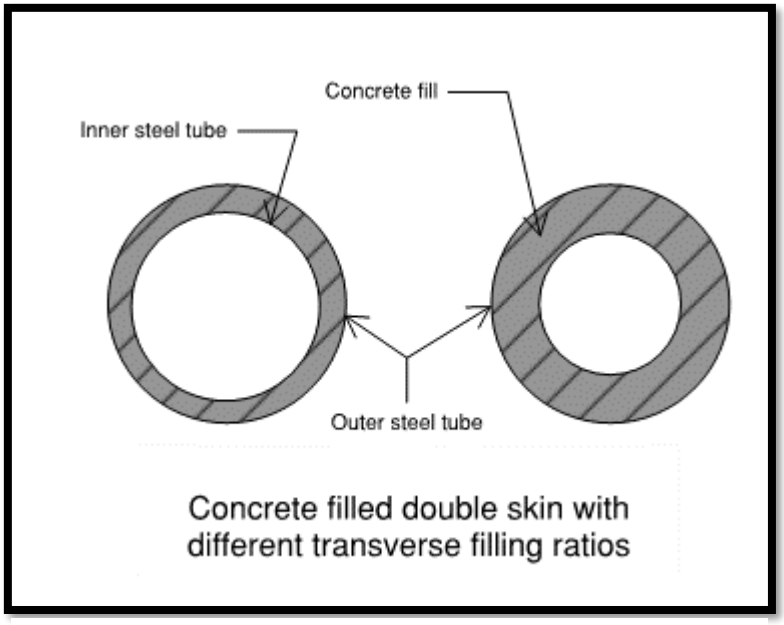

Figure 1: Transverse filling ratios

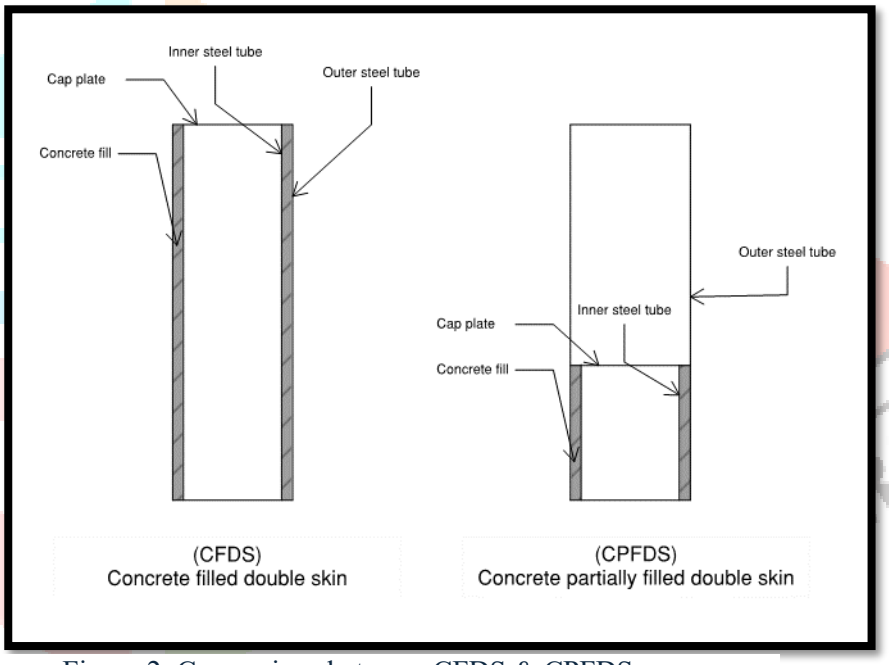

Figure 2: Comparison between CFDS & CPFDS.

2.0 Finite Element Model.

The finite element model for concrete-filled sections (CFS) and concrete-filled double-skin sections (CFDS) was developed and validated against prior experimental tests conducted under pure bending. The model was also verified using established equations designed to predict the capacity of both types of sections. Several key assumptions were incorporated to ensure the accuracy of the models and to effectively study the behavior of partially filled CFDS sections.

The following sections detail all the assumptions incorporated into the finite element model (FEM), providing a comprehensive overview of the considerations made to ensure accurate simulations and reliable predictions.

2.1 Material

The steel material was defined to simulate the elastic behavior of zero plastic strain with Young's modulus E = 2100000 Mpa, and a Poisson ratio of 0.3. a steel grade of S235 according to EN 10025: Hot Rolled Products of Structural Steels [7]. The assumed points for the non-linear engineering stress-strain curve are given in Table 1 as shown.

Table 1: The assumed Non-linear steel material properties (Engineering stress-strain).

	σ (Mpa)	**ε**
Pt 1	211.5	0
Pt 2	211.5	0.004
Pt 3	235	0.02
Pt 4	360	0.2

To capture the non-linearity of material the Engineering stress-strain curve into a true stress-strain curve as proposed with Faridmehr et al. [8] and the Abaqus Manual [9].

Engineering stress to true stress conversion formula:

$$\sigma_t = \sigma_e(1 + \epsilon_e) \qquad (2\text{-}1)$$

Engineering strain-to-strain conversion formula:

$$\epsilon_t = \ln(1 + \epsilon_e) \qquad (2\text{-}2)$$

The stress-strain curves used in the simulation were plotted as shown in Figure 3.

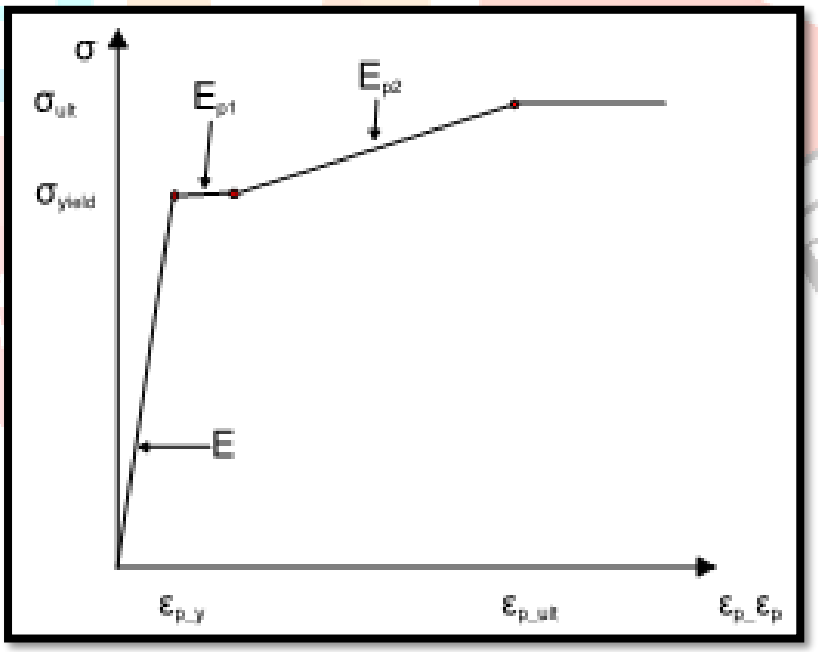

Figure 3: Stress-strain curve used in the simulation.

2.1.1 Concrete damaged plasticity model.

The concrete material is non-linear so to capture the cracking accurately, crushing of concrete and tension failure, the numerical computation proposed by Hafezolghorani et al. [10] was used for the concrete cube strength of 30 Mpa to express this non-linearity. A viscosity parameter of 0.007985 was assumed, the values used in the Abaqus model for the simulation of concrete damaged plasticity are given as shown in Table 2.

Table 2: The concrete damaged plasticity material properties values used.

Material's parameters	C30 (30 Mpa)	Plasticity parameters	
		Dilation angle	31
Concrete Elasticity		Eccentricity	0.1
E (GPa) Poisson ratio	26.6 0.2	fb0/fc0	1.16
		K	0.67
		Viscosity parameter	0.007985
Concrete compressive behavior		Concrete compression damage	
Yield stress (MPa)	Inelastic strain	Damage parameter C	Inelastic strain
15.3	0.0	0.00	0.0
19.2	0.000048249	0.00	0.000048249
22.5	0.000119844	0.00	0.000119844
25.2	0.000214786	0.00	0.000214786
27.3	0.000333074	0.00	0.000333074
28.8	0.000474708	0.00	0.000474708
29.7	0.000639689	0.00	0.000639689
30.0	0.000828016	0.00	0.000828016
29.7	0.001039689	0.01	0.001039689
28.8	0.001274708	0.04	0.001274708
27.3	0.001533074	0.09	0.001533074
25.2	0.001814786	0.16	0.001814786
22.5	0.002119844	0.25	0.002119844
19.2	0.002448249	0.36	0.002448249
15.3	0.002800000	0.49	0.002800000
10.8	0.003175097	0.64	0.003175097
5.7	0.003573541	0.81	0.003573541
Concrete tensile behavior		Concrete tension damage	
Yield stress (MPa)	Cracking strain	Damage parameter T	Cracking strain
3.0	0	0	0
0.03	0.001167315	0.99	0.001167315

The plasticity parameters can be defined as follows:

Dilation Angle: This angle represents the material's dilatancy, or the tendency to expand in volume when sheared. It is a measure of internal friction and is crucial for accurately modeling the behavior of concrete under load.

Eccentricity: This parameter defines the rate at which the hyperbolic flow potential approaches its asymptote in the p-q plane. It is a small positive number that influences the shape of the yield surface in the model.

fb0/fc0: This ratio represents the relationship between the initial equibiaxial compressive yield stress (fb0) and the initial uniaxial compressive yield stress (fc0). It helps in defining the yield surface for compressive loading conditions.

K: This parameter is often used to describe the ratio of the second stress invariant on the tensile meridian to that on the compressive meridian at initial yield. It is essential for defining the shape of the yield surface in the model.

2.2 Element type and mesh size:

The element type and mesh size play a crucial role in ensuring accurate results. Careful assumptions were made to capture the true behavior of the concrete, steel, and the interaction between both materials.

Mesh Element:

All three components, the outer steel tube, the concrete core, and the inner steel tube—were modeled using solid elements with their actual thicknesses. The element type used was C3D8I for all models.

Mesh size:

For the outer and inner steel tubes, a maximum mesh size of 10 mm was used. This fine meshing, as shown in Figure 4, was chosen to accurately capture local buckling effects, particularly in the outer steel tubes. For the concrete core, a maximum mesh size of 20 mm was applied to effectively capture the damaged regions of the mesh and ensure accurate simulation of the material behavior.

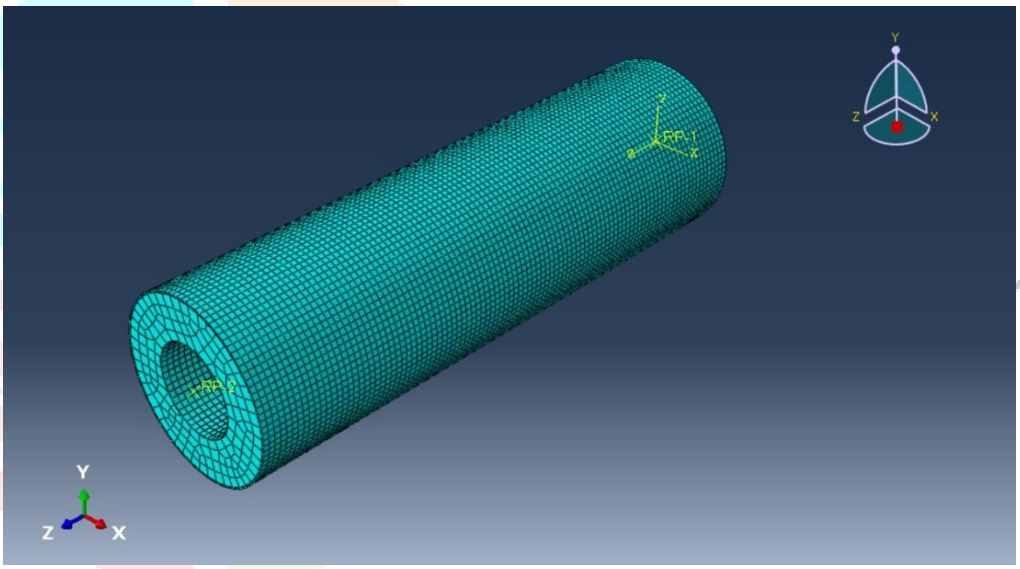

Figure 4: Meshing of a CFDS specimen.

2.3 Contact modelling:

For the interaction between the outer steel tube and the concrete, as well as the inner steel tube and the concrete, two contact properties were defined: **normal behavior** and **tangential behavior**. Based on the findings of Rabbat et al. [11], the coefficient of friction was assumed to be 0.65 for both contact surfaces.

2.4 Loading and boundary conditions.

The models of CFS or CFDS were simulated as cantilever beams as shown in Figure 5. A point load is acting at the other end of the beam using the general static method in loading.

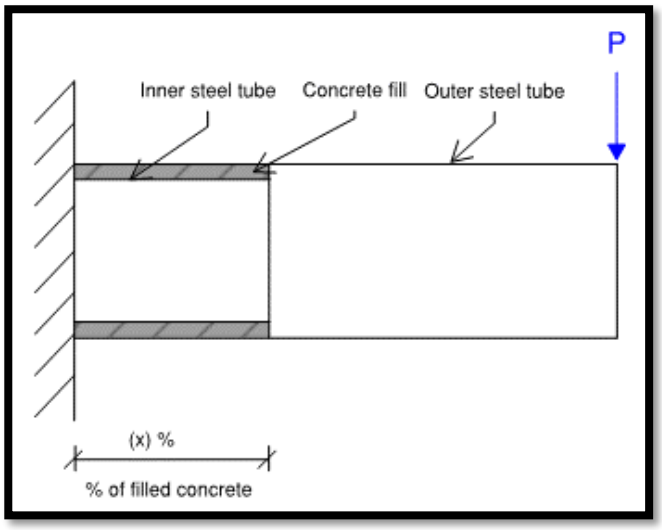

Figure 5:CFDS longitudinal filling ratios.

The fixed part is attached to a reference point in the centre of the tubes where the point is fixed for translation and rotations around the three axes, the point is attached to the surface of the end of the outer tube, inner tube and the concrete with ties where the surface nodes are attached with a rigid body, as shown in Figure 6.

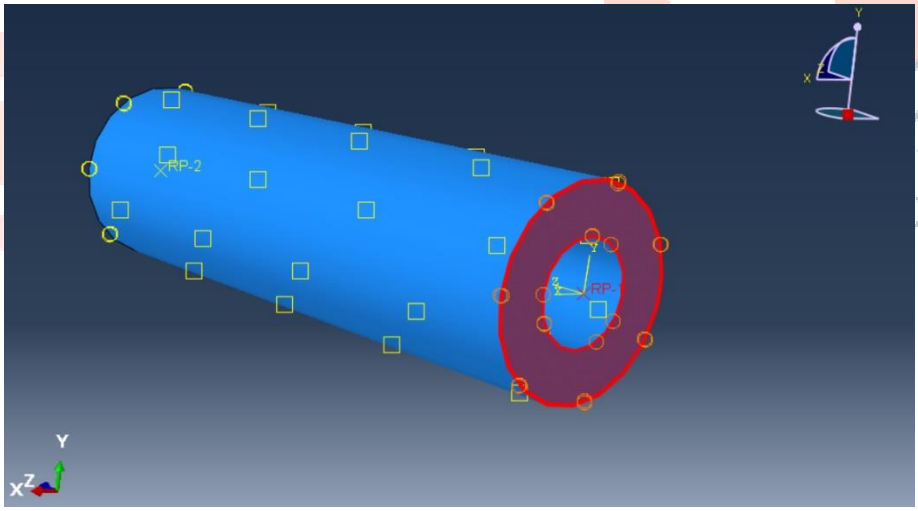

Figure 6: Interaction of the reference point to fixed side.

For the free end of the loading side, the surface of the outer skin tube only which is the thickness of the hollow tube attached with a rigid body and linked to a reference point in the centre of the tubes, and the load is applied as a point load on that reference point, as shown in Figure 7.

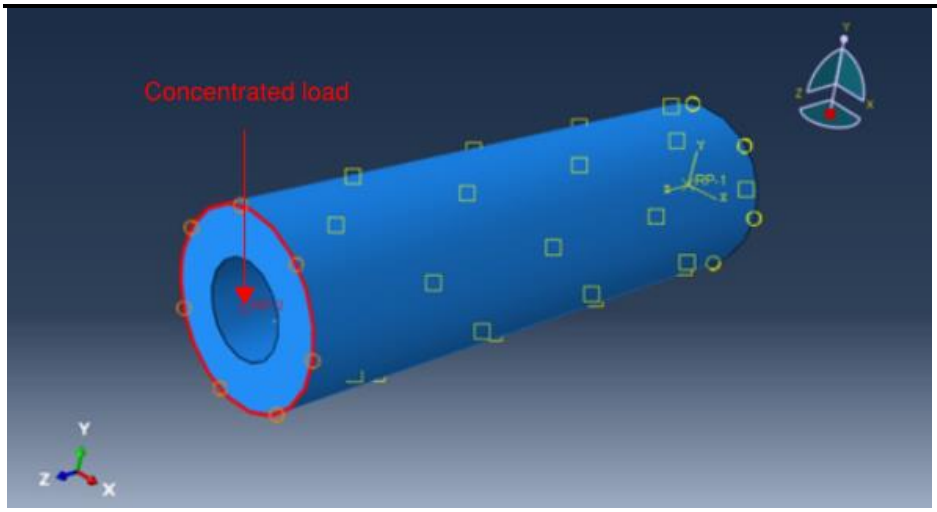

Figure 7:Interaction of the reference point to loading side.

2.5 Failure stopping criteria

in Abaqus, the default stopping criteria for a static general loading step are typically based on the maximum number of increments and the increment size, the maximum number of increments was maximized in all specimens in which that it is not governing in all models, where the minimum increment was specified as 1 Newton.

3.0 Finite Element Model Validation

The Validation of the FEM used was performed on both Concrete Filled tubes and then Concrete Filled Double Skin tubes to check the validity of the finite element model.

3.5.1 CFS Validation

The capacity of the CFS tube was calculated using equations from **CIDECT: Design Guide 5** [12]. The analysis was performed for tubes with a diameter of 300 mm and a thickness of 5 mm. A specimen length of 1000 mm was used in the calculations. The results are presented in **Table 3**.

Table 3: FEM values Vs CIDECT DG 5

Specimen	Calculated load CIDECT DG5 [12]	FEM (Load)	FEM/Calc. %
D300T5	127	120.1	0.95

The CFS tubes were also validated against experimental results for both fully filled and partially filled tubes, as presented by Khalifa et al. [3]. The results showed a good agreement with the experimental data, confirming the accuracy of the model, where the average ratio for the ultimate capacity of FEM to that of the experimental results is 105% with standard deviation of 14.6%.

Table 4: FEM values Vs Khalifa

Specimen	Expermintal load (KN) Khalifa et al. [3].	FEM (Load) (KN)	FEM/Exp. %
D114R100	12	11.19	93.3
D114R36	11.3	11.4	100.9
D114R16	9.1	11.05	121.4
		Average =	105.2
		S.D. =	14.6

The failure mode observed in the finite element models was consistent with the experimental results, as shown in **Figure 8** and **Figure 9**.

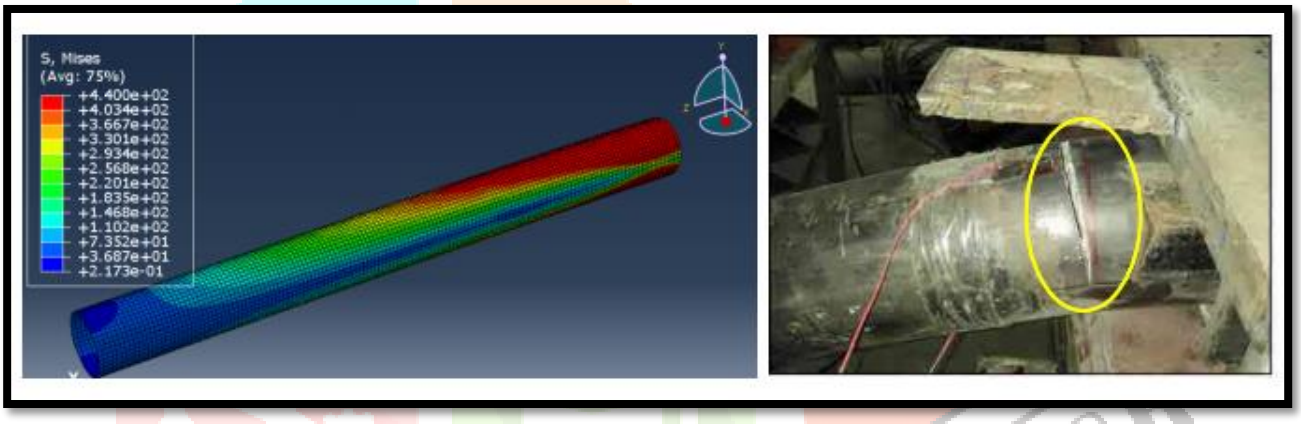

Figure 8: Tension Rupture failure mode FEM Vs experimental

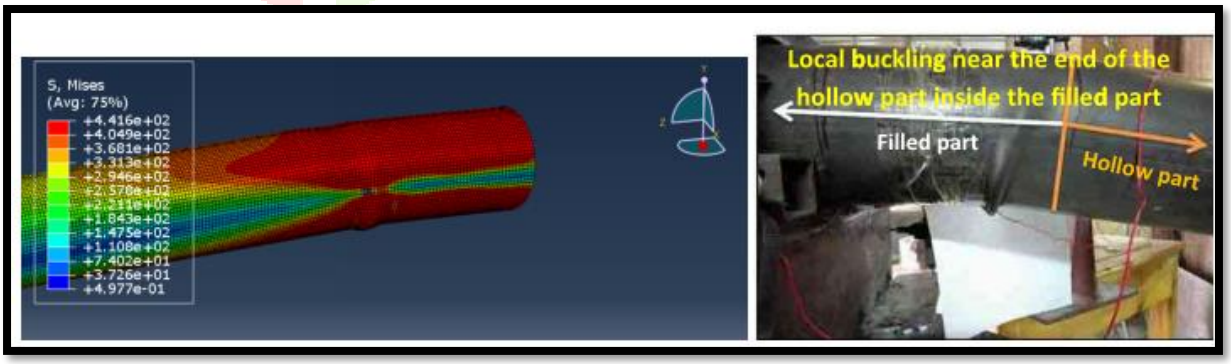

Figure 9: Local buckling failure mode FEM Vs experimental

3.5.2 CFDS Validation

For CFDS tube validation, Tao and Han [5] Proposed equations to calculate the capacity of the CFDS considering the confinement of concrete and failure load was considered at 1% strain. Table [5] shows a comparison between the FEM results and Tao and Han prediction considering the plastic section modulus. The average ratio for the ultimate capacity of FEM to that of the experimental results is 104.5% with a standard deviation of 3.9%.

Table 5: FEM values Vs TAO AND HAN

Specimen ID	FEM (Load)	Calculated load Tao and Han [5]	(FEM/Calculated load)%
DSPF-75Dt-50T-100L	148.2	138.75	106.8
DSPF-75Dt-60T-100L	141.57	133.47	106.1
DSPF-75Dt-70T-100L	143	125.09	114.3
DSPF-75Dt-80T-100L	122.73	112.9	108.7
DSPF-100Dt-50T-100L	117	109.1	107.2
DSPF-100Dt-60T-100L	103	104.31	98.7
DSPF-100Dt-70T-100L	97	96.85	100.2
DSPF-100Dt-80T-100L	88.6	86.2	102.8
DSPF-125Dt-50T-100L	94.8	90.93	104.3
DSPF-125Dt-60T-100L	88.3	86.6	102.0
DSPF-125Dt-70T-100L	80	79.8	100.3
DSPF-125Dt-80T-100L	72	70.3	102.4
DSPF-150Dt-50T-100L	90.5	83.77	108.0
DSPF-150Dt-60T-100L	80.7	78.5	102.8
DSPF-150Dt-70T-100L	73.4	70.7	103.8
DSPF-150Dt-80T-100L	62	59.9	103.5
		Average =	104.5
		S.D. =	3.9

The results from the FEM analysis models show a strong correlation between the experimental test outcomes and the theoretical predictions provided by the design equations. This alignment not only validates the accuracy of the FEM model but also reinforces its reliability in predicting the behavior of partially concrete-filled double-skin sections (PCFDS), as explored in this paper. This validation establishes a solid foundation for further research in this area.

4.0 Parametric study.

The study on partially concrete-filled double-skin sections (PCFDS) considers four different diameter-to-thickness ratios (D/t = 75, 100, 125, 150) and various transverse filling ratios (50%, 60%, 70%, 80%), analyzed in parallel with different longitudinal filling ratios (20%, 33%, 50%, 75%, 100%). **Figure 10** provides the model designation system used in this study.

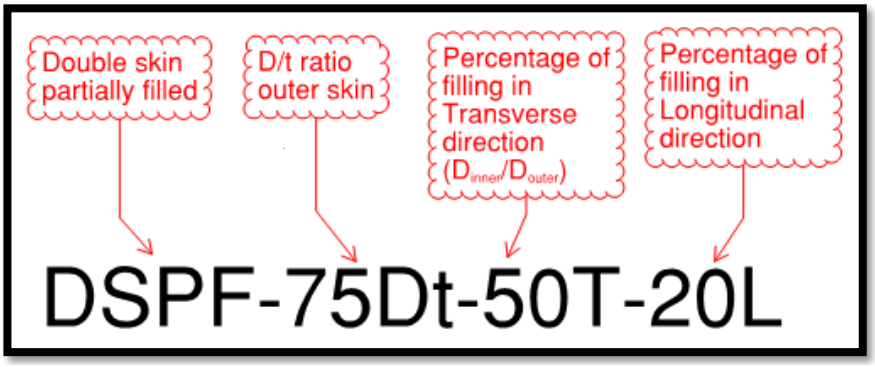

Figure 10: Specimen identification example.

All specimens were 1000 mm in length with an outer diameter of 300 mm and the thickness of the outer diameter varies to achieve the required D/t ratio. The inner diameter was kept constant to be 0.5 mm in all specimens.

4.1 Parametric study results

Figures 11 to 14 illustrate the relationship between the capacity ratio of the CFDS and the yield moment capacity of the outer tube against different longitudinal filling ratios. The capacity values for the fully filled CFS specimens, as per **CIDECT: Design Guide 5** [12], are also plotted on the same graph, using the same outer skin thickness for comparison.

Figure 11 illustrates the effect of the longitudinal filling ratio for models with D/t = 75. It shows that the capacity of the PCFDS increases significantly as the longitudinal filling ratio rises from 0% to 50% for different transverse filling ratios. However, further increases in the longitudinal filling ratio beyond 50% have a negligible effect on the capacity, except for the case with a 60% transverse filling ratio, where the capacity continues to increase up to a 100% longitudinal filling ratio.

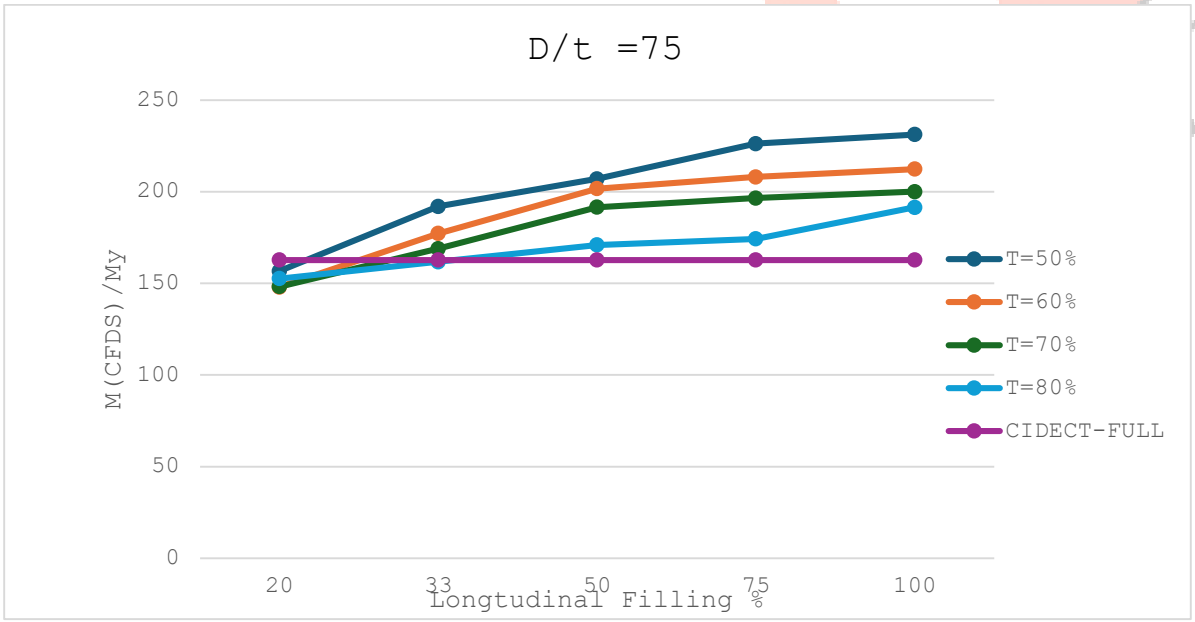

Figure 11: Moment capacity ratios for D/t=75.

Figures 12, 13, and 14 show the same behavior for different D/t ratios.

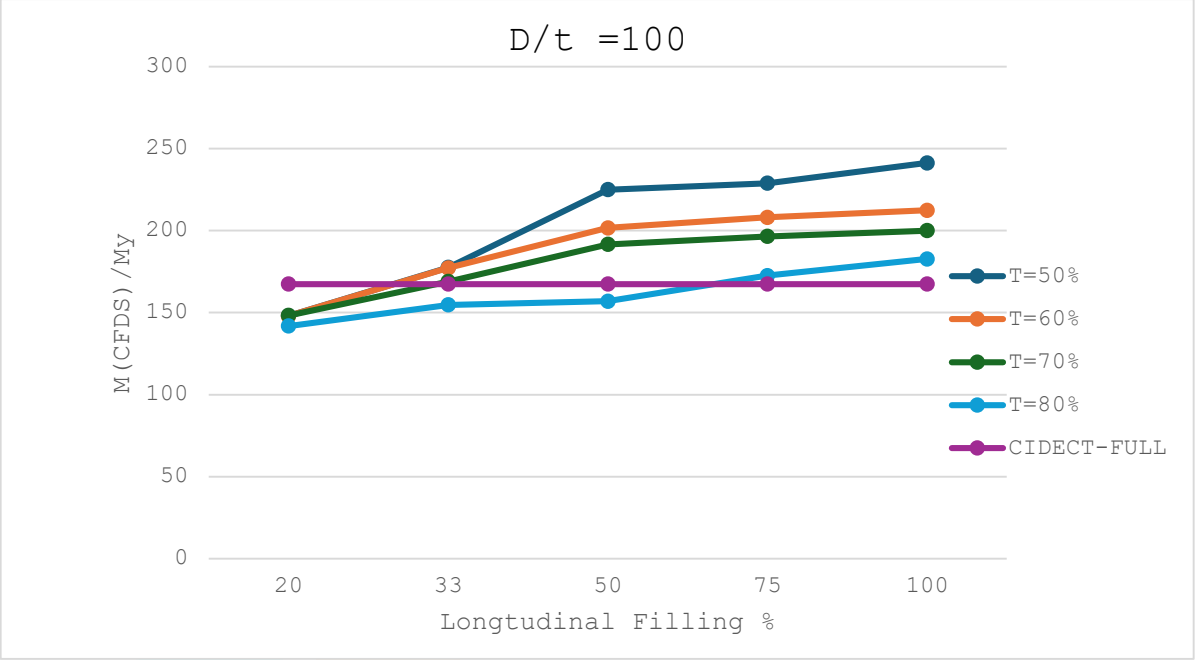

Figure 12: Moment capacity ratios for D/t=100.

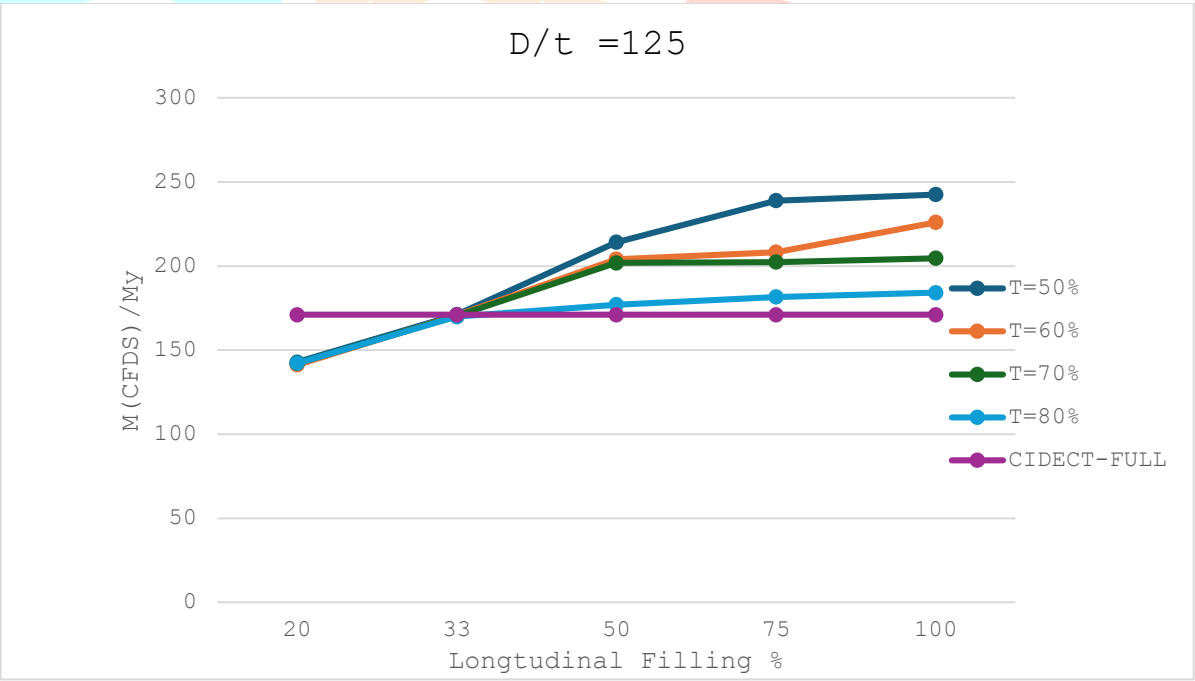

Figure 13: Moment capacity ratios for D/t=125.

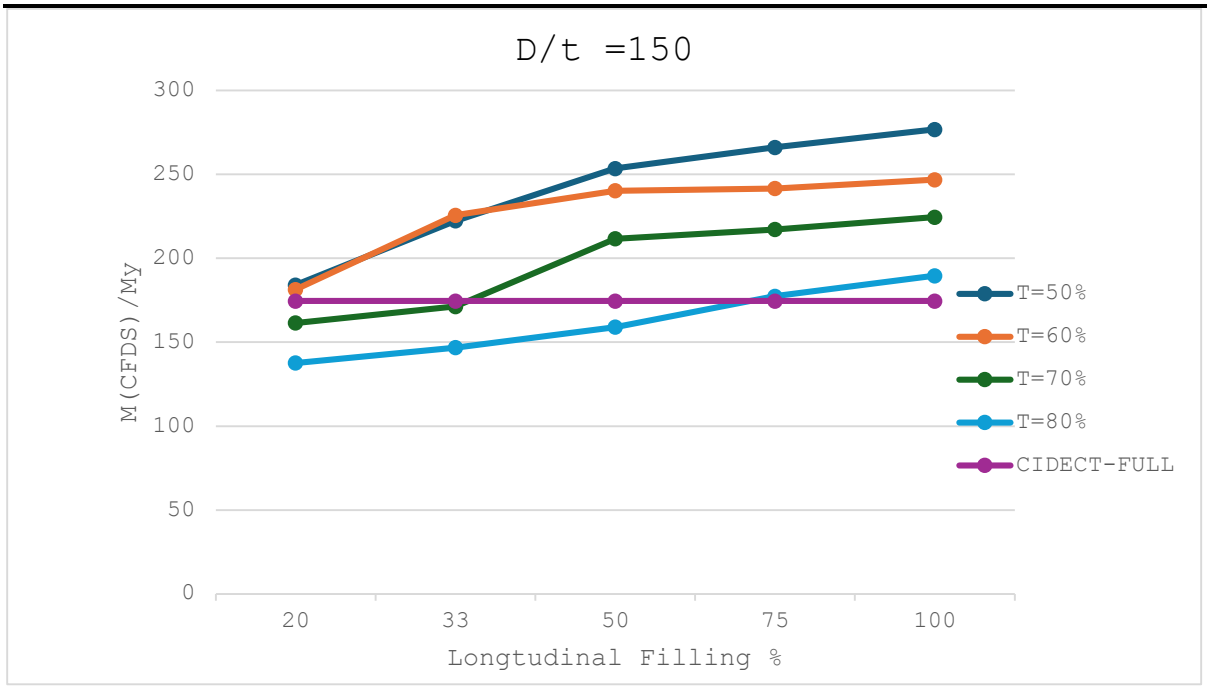

Figure 14: Moment capacity ratios for D/t=150.

The results indicate that the capacity of the partially concrete-filled double-skin (PCFDS) sections is generally higher than that of conventional concrete-filled steel (CFS) sections, as calculated using CIDECT guidelines. A significant gain in moment capacity can be achieved through partial concrete filling along the longitudinal direction. This optimized filling strategy allows for up to an 80% reduction in concrete volume compared to CFS sections while maintaining the same bending capacity

For partial filling ratios of less than 50% in the longitudinal direction, the failure mode was characterized by yielding at the termination point of the concrete filling, accompanied by local buckling in the compression zone at the same location, as shown in Figure 15.

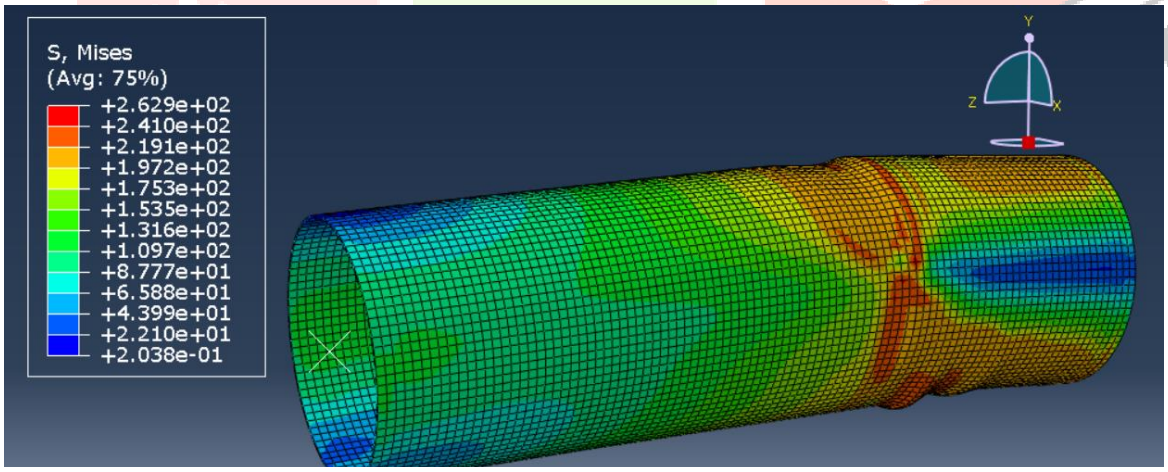

Figure 15: Failure for 33% longitudinal filling ratio. (Deformation x 10 times).

For a longitudinal filling ratio greater than 50%, the failure mode was characterized by yielding at the top fibers and local buckling at the bottom fibers, both occurring near the boundary condition, as illustrated in Figure 16

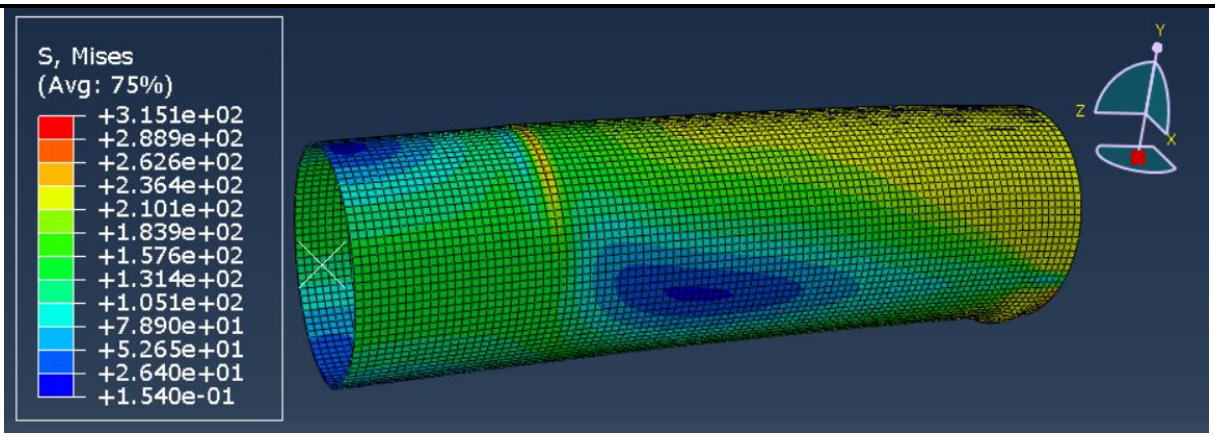

Figure 16: Failure for 75% longitudinal filling ratio. (Deformation x 10 times)

The results were collected and analyzed to develop an equation that provides a conservative estimate of the capacity of PCFDS. To ensure reliability and safety, a lower bound was incorporated into the equation to account for uncertainties and potential variations in material properties or construction methods.

5.0 Proposed Design Procedure.

The AISC360-22 [13] does not provide design procedures for the CFDS, where the capacity of the filled section in a longitudinal direction was proposed by Tao and Han [5].

The capacity was calculated as follows Mu depends on the capacity of the outer skin considering the yield strength, compressive strength of concrete, and the confinement made by the outer skin.

$$M_u = M_{osc,u} + M_{i,u} \quad (5\text{-}1)$$

$$M_{osc,u} = \gamma_m \cdot W_{scm} \cdot f_{scy} \quad (5\text{-}2)$$

$$\gamma_m = 1.04 + 0.48 \ln(\xi + 0.1) \quad (5\text{-}3)$$

Where the confinement factor is given by: $\xi = \frac{A_{so} \cdot f_{syo}}{A_{c,nominal} \cdot f_{ck}}$

$$W_{scm} = \frac{4}{3} \cdot (R_o^3 - R_i^3) \quad (5\text{-}4)$$

$$f_{scy} = C_1 X^2 \cdot C_2 (1.18 + 0.85\xi) \cdot f_{ck} \quad (5\text{-}5)$$

The coefficients C_1 and C_2 are calculated as follows:

$$C1 = \alpha / (1 + \alpha) \quad (5\text{-}6)$$

$$C2 = (1 + \alpha_{nominal}) / (1 + \alpha) \quad (5\text{-}7)$$

Where α and $\alpha_{nominal}$ are the steel ratio and nominal steel ratio, given by A_{so}/A_c and $A_{so}/A_{c,\,nominal}$ respectively. The units for f_{scy} and f_{ck} are N/mm^2.

The moment capacity of the inner tube is determined as follows:

$$M_{i,u} = W_{si} \cdot f_{syi} \quad (5\text{-}8)$$

Where W_{si} is the plastic section modulus of the inner tube.

The proposed equation to determine the capacity of the partial filling of concrete along the pipe is by multiplying the filled equation capacity by a modification factor as follows:

$$M_{n_{(longtudinal)}} = M.F \times M_{u_{(Tao\ and\ Han)}} \quad (5\text{-}9)$$

$$M.F = 1 + 0.2\ Ln\left(\frac{L_{filled}}{L_{full}}\right) \quad (5\text{-}10)$$

Where (L_{filled}) is the filling length of concrete in the longitudinal direction, and (L_{full}) is the filling length of the concrete and should be less than one. The transverse filling ratio was already considered in Tao and Han [5] equations. The comparisons between the proposed equations and the FEM model values were summarized and tabulated as shown in Tables 6 and 7

Table 6: Comparison between the FEM values and Design equations (D/t = 75,100)

	Mu (FEM) (KN.m)	**M (Eqn.) (KN.m)**	**M (Eqn) / M (FEM)**
DSPF-75Dt-50T-20L	100.43	94.09	0.937
DSPF-75Dt-50T-33L	123.04	107.98	0.878
DSPF-75Dt-50T-50L	132.67	119.52	0.901
DSPF-75Dt-50T-75L	145.00	130.77	0.902
DSPF-75Dt-50T-100L	148.20	138.75	0.936
DSPF-75Dt-60T-20L	99.36	90.51	0.911
DSPF-75Dt-60T-33L	100.70	103.88	1.032
DSPF-75Dt-60T-50L	118.41	114.97	0.971
DSPF-75Dt-60T-75L	135.50	125.79	0.928
DSPF-75Dt-60T-100L	141.57	133.47	0.943
DSPF-75Dt-70T-20L	99.23	84.83	0.855
DSPF-75Dt-70T-33L	120.00	97.35	0.811
DSPF-75Dt-70T-50L	135.00	107.75	0.798
DSPF-75Dt-70T-75L	142.50	117.89	0.827
DSPF-75Dt-70T-100L	143.00	125.09	0.875
DSPF-75Dt-80T-20L	97.80	76.56	0.783
DSPF-75Dt-80T-33L	103.70	87.87	0.847
DSPF-75Dt-80T-50L	109.60	97.25	0.887
DSPF-75Dt-80T-75L	111.70	106.40	0.953
DSPF-75Dt-80T-100L	122.73	112.90	0.920
DSPF-100Dt-50T-20L	71.80	73.98	1.030
DSPF-100Dt-50T-33L	86.10	84.91	0.986
DSPF-100Dt-50T-50L	109.10	93.98	0.861
DSPF-100Dt-50T-75L	111.00	102.82	0.926
DSPF-100Dt-50T-100L	117.00	109.10	0.932
DSPF-100Dt-60T-20L	71.75	70.73	0.986
DSPF-100Dt-60T-33L	85.95	81.18	0.945
DSPF-100Dt-60T-50L	97.80	89.85	0.919
DSPF-100Dt-60T-75L	100.90	98.31	0.974
DSPF-100Dt-60T-100L	103.00	104.31	1.013
DSPF-100Dt-70T-20L	71.90	65.68	0.913
DSPF-100Dt-70T-33L	81.92	75.38	0.920
DSPF-100Dt-70T-50L	92.90	83.42	0.898
DSPF-100Dt-70T-75L	95.30	91.28	0.958
DSPF-100Dt-70T-100L	97.00	96.85	0.998
DSPF-100Dt-80T-20L	68.80	58.45	0.850
DSPF-100Dt-80T-33L	75.04	67.09	0.894
DSPF-100Dt-80T-50L	76.10	74.25	0.976
DSPF-100Dt-80T-75L	83.70	81.24	0.971
DSPF-100Dt-80T-100L	88.60	86.20	0.973

Table 7:Comparison between the FEM values and Design equations (D/t = 125,150)

	Mu (FEM) (KN.m)	M (Eqn.) (KN.m)	M (Eqn) / M (FEM)
DSPF-125Dt-50T-20L	55.86	61.66	1.104
DSPF-125Dt-50T-33L	66.9	70.77	1.058
DSPF-125Dt-50T-50L	83.7	78.32	0.936
DSPF-125Dt-50T-75L	93.36	85.70	0.918
DSPF-125Dt-50T-100L	94.8	90.93	0.959
DSPF-125Dt-60T-20L	55.2	58.72	1.064
DSPF-125Dt-60T-33L	66.7	67.40	1.010
DSPF-125Dt-60T-50L	79.76	74.59	0.935
DSPF-125Dt-60T-75L	81.4	81.62	1.003
DSPF-125Dt-60T-100L	88.3	86.60	0.981
DSPF-125Dt-70T-20L	55.6	54.11	0.973
DSPF-125Dt-70T-33L	66.6	62.11	0.933
DSPF-125Dt-70T-50L	78.9	68.74	0.871
DSPF-125Dt-70T-75L	79.1	75.21	0.951
DSPF-125Dt-70T-100L	80	79.80	0.998
DSPF-125Dt-80T-20L	55.6	47.67	0.857
DSPF-125Dt-80T-33L	66.4	54.71	0.824
DSPF-125Dt-80T-50L	69.2	60.55	0.875
DSPF-125Dt-80T-75L	71	66.26	0.933
DSPF-125Dt-80T-100L	72	70.30	0.976
DSPF-150Dt-50T-20L	60.19	56.81	0.944
DSPF-150Dt-50T-33L	72.7	65.20	0.897
DSPF-150Dt-50T-50L	82.89	72.16	0.871
DSPF-150Dt-50T-75L	87	78.95	0.907
DSPF-150Dt-50T-100L	90.5	83.77	0.926
DSPF-150Dt-60T-20L	59.32	53.23	0.897
DSPF-150Dt-60T-33L	73.8	61.09	0.828
DSPF-150Dt-60T-50L	78.55	67.62	0.861
DSPF-150Dt-60T-75L	79	73.98	0.936
DSPF-150Dt-60T-100L	80.7	78.50	0.973
DSPF-150Dt-70T-20L	52.8	47.94	0.908
DSPF-150Dt-70T-33L	56	55.02	0.983
DSPF-150Dt-70T-50L	69.2	60.90	0.880
DSPF-150Dt-70T-75L	71	66.63	0.938
DSPF-150Dt-70T-100L	73.4	70.70	0.963
DSPF-150Dt-80T-20L	45	40.62	0.903
DSPF-150Dt-80T-33L	48	46.62	0.971
DSPF-150Dt-80T-50L	52	51.60	0.992
DSPF-150Dt-80T-75L	58	56.45	0.973
DSPF-150Dt-80T-100L	62	59.90	0.966

The comparisons revealed a strong alignment between the design equations and the FEM model values, demonstrating consistency across various D/t ratios. The results from the equations indicated that the lower bound was effectively achieved, confirming their reliability in predicting the capacity of partially concrete-filled double skin (PCFDS) structures. This solidifies the equations as dependable tools for accurate capacity prediction in these innovative structural systems.

6.0 Conclusion.

A finite element model (FEM) was developed based on the assumptions drawn from the conclusions of previous researchers to simulate the behavior of concrete-filled double-skin sections (CFDS) and concrete-filled sections (CFS). The FEM model was rigorously validated by comparing its results against both experimental test outcomes and the theoretical design equations proposed for CFS and CFDS structures. This validation ensures the accuracy and reliability of the model in predicting the behavior of these sections under various loading conditions.

The study focused on the partial concrete filling of double-skin partially concrete-filled double-skin (PCFDS) tubes in the longitudinal direction, which is a key parameter in optimizing the strength-to-weight ratio and capacity of such structural elements. The parametric study covered a wide range of scenarios, examining various diameter-to-thickness (D/t) ratios alongside different transverse filling ratios. These ratios were selected to explore the combined effects of filling both longitudinal and transverse directions on the overall performance of the PCFDS structures.

The findings from the parametric study demonstrated that the capacity of the PCFDS structures increased significantly as the longitudinal filling ratio increased from 0% to 50%. However, after the 50% longitudinal filling threshold, further increases in the filling ratio yielded diminishing returns, with the capacity increase becoming negligible. This behavior was consistent across the various D/t ratios and transverse filling ratios studied, except for the case with a 60% transverse filling ratio. In this specific case, the gain in capacity continued to increase as the longitudinal filling ratio exceeded 50%, indicating a unique interaction between the longitudinal and transverse filling ratios at this specific point. The saving of the concrete of PCFS from CFS can reach up to 80% save in concrete volume with the same bending capacity.

To provide a more practical and generalizable method for predicting the capacity of PCFDS under varying filling conditions, a modification factor was proposed. This modification factor enables the prediction of the capacity at any specific longitudinal filling ratio by multiplying it with the capacity of the fully concrete-filled double skin section (CFDS). This factor serves as a useful tool for engineers and designers, offering a simple and effective way to estimate the strength of partially concrete-filled double-skin sections without needing extensive recalculations for each possible filling ratio.

8. Annotations

$A_{c,nominal}$	Nominal cross-sectional area of concrete, equal to the void area inside the outer steel tube
A_{so}	Cross-sectional area of the outer steel tube
CFS	Concrete Filled sections
CFDS	Concrete Filled Double Skin
E	Modulus of elasticity
f_{syo}	Yield strength of the outer steel tube
f_{ck}	Characteristic concrete strength (= 0.67. f_{cu})
f_{syi}	Yield strength of the inner steel tube
f_{cu}	Characteristic cube strength of concrete
L_{filled}	The length of the partial filling of concrete.
L_{full}	The length of the whole member of the concrete filled double skin.
M_u	Ultimate strength of the CFDST beams
$M_{i,u}$	Moment capacity of the inner tube
$M_{n_{(longtudinal)}}$	The nominal moment capacity for the partial concrete filled double skin.
PCFDS	Partially Concrete-Filled Double-Skin Sections
R_o	Radius of the outer steel tube
R_i	Radius of the inner steel tube
W_{scm}.	Plastic section modulus of the outer steel tube and the and sandwiched concrete.
W_{si}	Plastic section modulus of the inner tube
X	Hollow section ratio, given by Hollow section ratio, given by = $\frac{R_i}{R_o}$
σ_e	Engineering stress
ϵ_t	True strain
ϵ_e	Engineering strain
σ_t	True stress
ξ	Confinement factor

9.0 References

1. Moon, J., et al., Analytical modeling of bending of circular concrete-filled steel tubes. 2012. **42**: p. 349-361.
2. Lu, H., L.-H. Han, and X.-L.J.T.-W.S. Zhao, Analytical behavior of circular concrete-filled thin-walled steel tubes subjected to bending. 2009. **47**(3): p. 346-358.
3. Khalifa, M., A. Shaat, and S. Ibrahim, Optimum concrete filling ratio for partially filled noncompact steel tubes. Thin-Walled Structures, 2019. **134**: p. 159-173.
4. (AISC), A.I.o.S.C., Specification for Structural Steel Buildings. ANSI/AISC 360-10 ed. 2010, Chicago, IL: American Institute of Steel Construction.
5. Tao, Z. and L.-H.J.J.o.C.S.R. Han, Behaviour of concrete-filled double skin rectangular steel tubular beam–columns. 2006. **62**(7): p. 631-646.
6. Huang, H., L.-H. Han, and X.-L.J.J.o.C.S.R. Zhao, Investigation on concrete filled double skin steel tubes (CFDSTs) under pure torsion. 2013. **90**: p. 221-234.
7. (CEN), E.C.f.S., EN 10025: Hot Rolled Products of Structural Steels. Vol. Part 2, 3, 4 and 6.: CEN.
8. Faridmehr, I., et al., Correlation between engineering stress-strain and true stress-strain curve. 2014. **2**(1): p. 53-59.
9. Corp, D.S.S., ABAQUS/Standard User's Manual, Version 6.9. United States: Dassault Systèmes Simulia Corp.
10. Hafezolghorani, M., et al., Simplified damage plasticity model for concrete. 2017. **27**(1): p. 68-78.
11. Rabbat, B.G. and H.G. Russell, Friction Coefficient of Steel on Concrete or Grout. 1985. **111**(3): p. 505-515.
12. Structures), C.I.C.f.t.D.a.S.o.T., Design Guide 5: Construction with Hollow Steel Sections. CIDECT.
13. (AISC), A.I.o.S.C., Specification for Structural Steel Buildings. ANSI/AISC 360-22 ed. 2022, Chicago, IL: American Institute of Steel Construction.